Enzymes

How to cite:
International Edition: doi.org/10.1002/anie.202008444
German Edition: doi.org/10.1002/ange.202008444

Outer-Membrane Protease (OmpT) Based *E. coli* Sensing with Anionic Polythiophene and Unlabeled Peptide Substrate

*Gaurav Sinsinbar[+], Sushanth Gudlur[+], Sarah E. Wood, Gopal Ammanath, Hakan U. Yildiz, Palaniappan Alagappan, Milan Mrksich, and Bo Liedberg**

Abstract: *E. coli and Salmonella are two of the most common bacterial pathogens involved in foodborne and waterborne related deaths. Hence, it is critical to develop rapid and sensitive detection strategies for near-outbreak applications. Reported is a simple and specific assay to detect as low as 1 CFU mL^{-1} of E. coli in water within 6 hours by targeting the bacteria's surface protease activity. The assay relies on polythiophene acetic acid (PTAA) as an optical reporter and a short unlabeled peptide ($LL37_{FRRV}$) previously optimized as a substrate for OmpT, an outer-membrane protease on E. coli. $LL37_{FRRV}$ interacts with PTAA to enhance its fluorescence while also inducing the formation of a helical PTAA-$LL37_{FRRV}$ construct, as confirmed by circular dichroism. However, in the presence of E. coli $LL37_{FRRV}$ is cleaved and can no longer affect the conformations and optical properties of PTAA. This ability to distinguish between an intact and cleaved peptide was investigated in detail using $LL37_{FRRV}$ sequence variants.*

Introduction

Escherichia coli and *Salmonella enterica* are two of the most common bacterial pathogens involved in foodborne and waterborne related deaths around the world.[1] According to the most recent WHO report on foodborne illnesses, nearly 0.42 million people worldwide die annually of preventable diarrheal infections caused by ingesting contaminated food and water.[1] Among all causative agents spanning microbial, parasitic, and chemical origins, *E. coli* and *Salmonella* are the leading causes of such deaths. Along with implementing rigorous food and water safety standards, an early detection of bacterial contamination in water and food sources could help contain, control, and prevent *E. coli*, *Salmonella*, and other bacterial outbreaks.

Conventional methods, considered to be gold standards, for detecting bacterial pathogens require pre-processing of samples, bacterial culturing, and subsequent biochemical assays.[2,3] This is time-consuming, labor-intensive, and requires a trained technician to perform the assays. Various rapid detection methods have been developed based on nucleic acid amplification and immunoassays, but these techniques are laboratory-based that require specialized instruments and a trained user, which are usually out of reach for resource-limited communities.[2,4]

In the present study, we have developed a simple functional assay for detecting *E. coli* in water samples that avoids labor-intensive steps involved in DNA/RNA isolation for nucleic acids assays and circumvents stability and storage issues commonly faced with antibodies in immunoassays. It involves measuring changes in optical properties of a polythiophene (PT) reporter when mixed with an unlabeled peptide substrate specifically designed and optimized for an *E. coli* outer-membrane protease (Figure 1). To the best of our knowledge, this is the first time an outer-membrane protease has been targeted to develop a functional assay for detecting bacterial pathogens using unlabeled peptide substrates. Using this method, we were able to achieve a detection limit of 1 CFU mL^{-1} in 6 h with a pre-culturing step and 10^5 CFU mL^{-1} in 1 h without any pre-culturing. The low detection limit and short assay time are better than most commercially available detection kits for *E. coli*.

The method described in this article relies on the enzymatic activity of OmpT, a membrane protease present on the surface of all wild-type *E. coli* strains.[5–7] OmpT is known to cleave short peptides preferentially at dibasic sites (-K-K-, -K-R-, -R-K-, and –R-R-).[7,8] It acts as a defense mechanism for *E. coli* by cleaving cationic Anti-Microbial Peptides (cAMPs) that are secreted by the human body as a defense mechanism against bacterial pathogens.[9,10]

Previously, we optimized a short peptide sequence at the preferred cleavage site for OmpT by screening a library of 364 peptides using self-assembled monolayers for matrix-assisted laser-desorption-ionization mass spectrometry (SAMDI-MS), a high throughput mass spectrometry technique.[11] The optimized tetrapeptide sequence, FRRV was substituted into a 15-residue peptide fragment derived from the N-terminal region of the longer LL37 peptide, a well-known cAMP.[12–14] For the optimized substrate with the sequence CLLGDF**FRRV**KEKIG ($LL37_{FRRV}$), OmpT exhibited a catalytic efficiency that was 400 times higher than what was

[*] Dr. G. Sinsinbar,[+] Dr. S. Gudlur,[+] Dr. G. Ammanath, Dr. P. Alagappan, Prof. B. Liedberg
Centre for Biomimetic Sensor Science, School of Materials Science Engineering, Nanyang Technological University
50 Nanyang Drive, Singapore, 637553 (Singapore)
E-mail: bliedberg@ntu.edu.sg
Dr. S. E. Wood, Prof. M. Mrksich
Departments of Chemistry and Biomedical Engineering, Northwestern University, 2145 Sheridan Road, Evanston, IL 60208 (USA)
Dr. H. U. Yildiz
Department of Chemistry, Izmir Institute of Technology
Urla, 35430, Izmir (Turkey)
[+] These authors contributed equally to this work.
Supporting information and the ORCID identification number(s) for the author(s) of this article can be found under: https://doi.org/10.1002/anie.202008444.

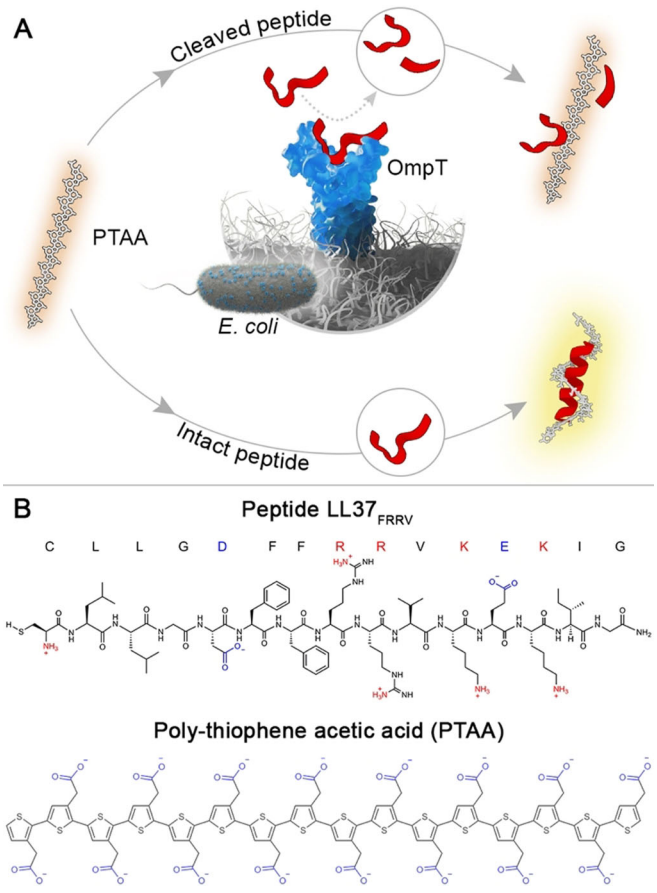

Figure 1. OmpT-based *E. coli* sensing. A) Schematic illustration of OmpT-based *E. coli* sensing with anionic polythiophene and unlabeled peptide substrate. B) Chemical structures of the unlabeled peptide ($LL37_{FRRV}$) and the anionic polythiophene (PTAA). Red or blue color highlights positive or negative ionizable groups, respectively. Experimental procedures and characterization tools are described in the materials and methods section (Supporting Information).

observed for the native LL37 fragment with the sequence CLLGDF**FRRS**KEKIG.[11] Hence, we have used $LL37_{FRRV}$ as the preferred peptide substrate in this study (Figure 1B).

For reporting, we chose PTAA, an anionic PT with a carboxyl functional group, designed to interact with the positively charged residues on $LL37_{FRRV}$ (Figure 1B). PTs constitute a class of conjugated conducting polymers and have found applications in many chemical- and bio-sensing platforms in the recent past.[15,16] The optical properties of PTs depend on the conformation of the polymer backbone.[17–19] Hence, the optical properties can be tuned by modifying the side chains with different functional groups. These functional groups can interact with DNA, protein, peptides, small bioanalytes, metal ions, and surfactants resulting in changes in structural, electronic, and optical properties of the PT.

Upon mixing PTAA with intact $LL37_{FRRV}$, the PTAA undergoes a conformational change causing an increase in its fluorescence. However, mixing PTAA with the cleaved fragments of $LL37_{FRRV}$ resulting from OmpT digestion does not cause a conformational change in PTAA and hence, no fluorescence increase is observed. This ability of PTAA to distinguish between an intact $LL37_{FRRV}$ and its cleaved fragments, which was studied in great detail herein by screening peptide sequence variants of $LL37_{FRRV}$, is the basis for detecting *E. coli* in water samples. In the first step of the assay, $LL37_{FRRV}$ is added to an aqueous sample suspected of *E. coli* contamination and the sample incubated for sufficient time. In the second and final step, PTAA is added to the sample and the fluorescence intensity measured. An increase in PTAA fluorescence, when compared to a control, indicates the absence of *E. coli* while no change in PTAA fluorescence confirms the presence of *E. coli* (Figure 1A).

Results and Discussion

Interaction between PTAA and Intact/Cleaved $LL37_{FRRV}$

PTAA in an alkaline buffer has an absorption maximum at 450 nm (Figure 2A black) and upon mixing with $LL37_{FRRV}$ exhibits a blue shift (Figure 2A). This blue shift increases with increasing peptide concentration until it saturates at $\approx 50\ \mu M$ of the added peptide (Figure 2A dark blue). At sufficiently high PTAA and peptide concentrations, a corresponding color change can be detected with the naked eye (Figure S1). When excited at 420 nm, PTAA exhibits a fluorescence emission maximum at 550 nm (Figure 2B black). Upon mixing with $LL37_{FRRV}$, the fluorescence intensity at 550 nm increases linearly with increasing peptide concentration until it saturates at $\approx 50\ \mu M$ of the added peptide (Figure 2B dark blue & 2C) and represents the highest point in the linear dynamic range. Hence, 50 μM was chosen for further experiments in order to have a larger working window for measuring changes in fluorescence intensity. Furthermore, the maximum increase in PTAA's fluorescence intensity upon peptide addition was close to 200% (Figure 2C).

The changes observed in the optical properties of PTAA alone and when mixed with $LL37_{FRRV}$ can be understood by examining the polymer's conjugation system at the molecular level. PTAA has a π-conjugated polymer backbone which is effective in the delocalization of π-electrons along the polymer chain, and thus giving rise to its photoluminescence. One of the requirements for conjugation is the overlap of π-orbitals, implying that the conjugated system should be planar. The conjugation length is determined by the number of coplanar rings, and a longer conjugation length shifts the absorption spectrum towards longer wavelengths. Thus, PTAA's initial absorbance maximum at 450 nm (Figure 2A black) represents planarization and stretching of the polymer backbone (Figure 2D Planar PTAA).[17,18,20] This planar conformation of PTAA's backbone is stabilized by electrostatic repulsion between the deprotonated carboxylic groups in the side chains. Planar PTAAs also could be grouped together showing non-radiative de-excitation because of the contact between the polymer chains, which contributes to a lowering of its fluorescence intensity.[17] Importantly, PTAA and other conjugated systems are known to undergo reversible planar to nonplanar conformational transitions causing the overall conjugation length to decrease or increase, respectively, thus affecting PTAA's optical properties.[21,22]

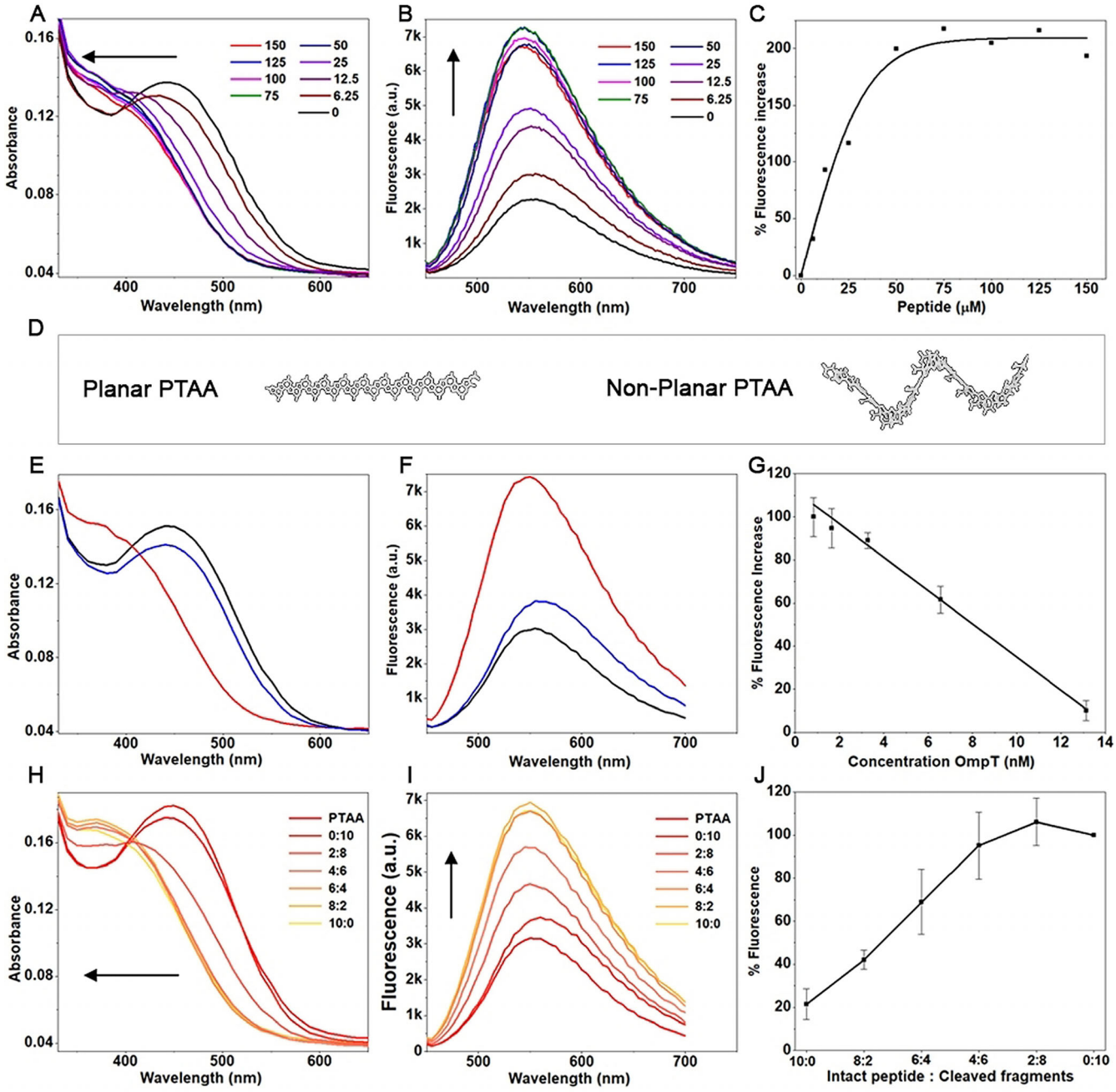

Figure 2. Absorption and fluorescence spectra of PTAA and PTAA-LL37$_{FRRV}$ complex. A) Absorption spectra and B) Fluorescence spectra of PTAA exhibiting a blue shift and an increase in fluorescence intensity, respectively, that corresponds to increasing LL37$_{FRRV}$ concentrations. C) Increase in fluorescence intensity of PTAA at 550 nm when mixed with increasing concentrations of intact LL37$_{FRRV}$. D) Cartoon of proposed models of the planar and nonplanar conformations, here exemplified with a helical backbone which is one of the many different possible nonplanar conformations of PTAA. E) Absorption spectra and F) fluorescence spectra of PTAA (black), PTAA mixed with intact LL37$_{FRRV}$ (red), and PTAA mixed with LL37$_{FRRV}$ treated with OmpT (blue). G) Change in PTAA fluorescence intensity at 550 nm when mixed with 50 μM LL37$_{FRRV}$ previously treated with varying concentrations of OmpT for 2 h. H) Absorption spectra and I) fluorescence spectra of PTAA when mixed with different ratios of intact and cleaved synthetic LL37$_{FRRV}$ fragments exhibiting a blue shift that corresponds to decreasing conjugation length with increasing fraction of LL37$_{FRRV}$ concentrations. Black arrow indicates the direction of decrease in conjugation length. J) Fluorescence intensity of PTAA at 550 nm when mixed with different ratios of intact and cleaved synthetic LL37$_{FRRV}$ fragments. Error bars in G & J represent standard error of the mean for $n = 3$. Black line in C and G are nonlinear (dose-response) and linear fit of the data, respectively.

A variety of environmental factors can cause the conjugated backbone to transition from a planar to nonplanar conformation including temperature, solvent, an electric field, and dissolved ions.[17,23–25] In the case of PTAA-peptide interactions, the principal molecular forces influencing the conformational change of the polymer backbone are electrostatic interactions, hydrogen bonding, and to a smaller extent nonpolar interactions.[26–29] LL37$_{FRRV}$ carries two arginines

(R) and two lysines (K) in its sequence (Figure 1B) whose side chains carry a positively charged amine group capable of interacting electrostatically with the negatively charged carboxyl group of the polymer side chains. The attractive electrostatic interaction between the peptide and polymer will force the polymer chains to separate and induce a chirality in its backbone[18,20] (Figure 2D Nonplanar PTAA), and this is confirmed by circular dichroism (CD) measurements as described below. Thus, the PTAA-$LL37_{FRRV}$ interaction will decrease the effective conjugation length of the polymer backbone,[18,28] which in turn leads to a blue shift in its absorption spectrum (Figure 2A) and a concomitant increase in its fluorescence emission (Figure 2B&C).

In the following sections we investigate the influence of the peptide length, peptide net charge, peptide charge distribution, and secondary conformations on the optical properties of PTAA.

Effect of Peptide Length on the Optical Properties of PTAA

$LL37_{FRRV}$ is a substrate for OmpT (Figure S2) and it cleaves the peptide at its dibasic site (-R_8-R_9-) to yield two short fragments of eight and seven residues, which was confirmed by MALDI-TOF analysis with peaks at 970 and 828 *m*/*z*, respectively (Table S1 and Figure S5). When $LL37_{FRRV}$ that was first treated with recombinant OmpT for two hours at 37 °C and then mixed with PTAA, we could neither detect any blue shift in absorption (Figure 2E blue) nor any significant increase in fluorescence intensity (Figure 2F blue). End-point fluorescence intensity measurements of PTAA when mixed with 50 μM of $LL37_{FRRV}$ incubated with varying concentrations of OmpT (0.8–13.1 nM) revealed an overall decrease in PTAA's fluorescence intensity that correlated with increasing OmpT concentration (Figure 2G). For samples with an OmpT concentration above ≈13 nM, the increase in PTAA fluorescence intensity was no more than ≈10%, suggesting that almost all of the $LL37_{FRRV}$ was cleaved into shorter fragments that did not significantly contribute to PTAA fluorescence (Figure 2G).

To further confirm that the cleaved peptide fragments did not contribute significantly towards changing the optical properties of PTAA, we separately synthesized two short peptides ($_{frag1}LL37_{FRRV}$ and $_{frag2}LL37_{FRRV}$) that were identical to the two cleaved fragments obtained when OmpT cleaves $LL37_{FRRV}$ (Table S1). When $_{frag1}LL37_{FRRV}$ and $_{frag2}LL37_{FRRV}$ were mixed with PTAA, they did not result in a blue shift in PTAA absorption (Figure 2H 0:10 Intact:Cleaved). Nor did they induce a significant increase in PTAA fluorescence (Figure 2I 0:10). However, when $_{frag1}LL37_{FRRV}$ and $_{frag2}LL37_{FRRV}$ were combined with intact $LL37_{FRRV}$ in different ratios, while keeping the total peptide concentration same, and subsequently mixed with PTAA, blue shifts in absorption (Figure 2H 2:8–8:2) and significant fluorescence intensity changes (Figure 2I 2:8–8:2) were observed in agreement with a change in conformation and an overall decrease in conjugation length of the PTAA backbone.

Even though the total peptide concentration remained same in all the samples, the magnitude of change in PTAA's optical properties was directly proportional to the amount of intact peptide in the sample (Figure 2H–J), suggesting that peptide length is a major contributing factor in affecting PTAA's optical properties. It is still too early to rule out the possibility that the cleaved peptide fragments interact locally with PTAA and induce small twists along its backbone. However, such local perturbations appear insufficient to induce a major change in PTAA's optical properties. Thus, the length of the peptide clearly is an important factor affecting PTAA backbone chirality and conjugation length. Similar observations related to optical property changes were reported by Chen et al. (2012),[30] Inganäs and co-workers (2005),[31,32] and Rubio-Magnieto et al. (2015)[33] for cationic PTs interacting with intact or cleaved DNA oligonucleotides. They reported that the interaction between cationic PT and dsDNA was distinguishable from PT's interaction with ssDNA, including those that resulted from the Pb^{2+} induced DNAzyme digestion of dsDNA by Chen et al. (2012).[30] Despite the net charge of the sample remaining unchanged, they observed a difference in fluorescence intensity that was attributed to a change in the π-electron overlap which altered the effective conjugation length of the polymer.[31,32] Similar to the data presented here for the interaction between PTAA and intact/cleaved $LL37_{FRRV}$, the cationic PTs exhibited different fluorescence spectra when free in solution, bound to ssDNA, or bound to dsDNA.[30–33] Moreover, the magnitude of the change in PT's fluorescence was found to be dependent on the ssDNA sequence, length, and topology.[33]

Effect of Peptide's Net Positive Charge and Charge Distribution on PTAA Fluorescence

In order to appraise the role of peptide's positive charges in affecting PTAA fluorescence, $LL37_{FRRV}$ sequence was modified to vary its overall net charge from 0 to +3 while keeping the total number of residues constant. The resulting six $LL37_{FRRV}$ peptide variants were designed by substituting one or both lysine residues with alanines and by either modifying the N-terminal ionizable group with an acetyl cap or leaving it unmodified (Table 1 ID 1–6). The optimized FRRV sequence, carrying the critical dibasic site recognized by OmpT, was not altered so as to preserve the peptide's fundamental utility in the "OmpT-PTAA assay" (described below).

When mixed with increasing concentrations (0.4–100 μM) of the six $LL37_{FRRV}$ peptide variants (Table 1, ID 1–6), PTAA exhibited a concomitant increase in fluorescence until the fluorescence intensity reached a maximum (Figure S3.I A&B). Once PTAA reached its maximum fluorescence, addition of any more peptide resulted in either no change in fluorescence (Figure S3.I A squares and circles) or a slight decrease in fluorescence intensity due to peptide-induced PTAA aggregation (Figure S3.I B squares). Thus, irrespective of the net charge, all six $LL37_{FRRV}$ peptide variants caused an increase in PTAA fluorescence; however, the peptide concentration at which PTAA reached its maximum fluorescence intensity was dependent on the peptide's net charge (Figure S3.I A&B). Peptides with a higher net charge (Figure S3.I

Table 1: List of $LL37_{FRRV}$ peptide variants with differing net charge of intact (a) and cleaved fragments (*b*).

ID	Peptide Sequence	*a*	*b*	Cleaved Fragments
1	Ac-CLLGDFFRRV**A**E**A**IG-NH_2	0	−1	Ac-CLLGDFFR-COO^-
			+1	$^+NH_3$-RV**A**E**A**IG-NH_2
2	Ac-CLLGDFFRRV**K**E**A**IG-NH_2	+1	−1	Ac-CLLGDFFR-COO^-
			+2	$^+NH_3$-RV**K**E**A**IG-NH_2
3	Ac-CLLGDFFRRV**K**E**K**IG-NH_2	+2	−1	Ac-CLLGDFFR-COO^-
			+3	$^+NH_3$-RV**K**E**K**IG-NH_2
4	$^+NH_3$-CLLGDFFRRV**K**E**K**IG-NH_2	+3	0	$^+NH_3$-CLLGDFFR-COO^-
			+3	$^+NH_3$-RV**K**E**K**IG-NH_2
5	$^+NH_3$-CLLGDFFRRV**K**E**A**IG-NH_2	+2	0	$^+NH_3$-CLLGDFFR-COO^-
			+2	$^+NH_3$-RV**K**E**A**IG-NH_2
6	$^+NH_3$-CLLGDFFRRV**A**E**A**IG-NH_2	+1	0	$^+NH_3$-CLLGDFFR-COO^-
			+1	$^+NH_3$-RV**A**E**A**IG-NH_2

A&B squares, ID 3&4 in Table 1) caused PTAA to exhibit maximum fluorescence at a relatively lower concentration than peptides with lower net charge (Figure S3.I A&B triangles, ID 1&6 in Table 1). Thus, for a given peptide concentration, PTAA's fluorescence intensity positively correlated with the peptide's net charge as seen in Figure 3A where 6.25 μM (a data point within the linear response, Figure S3.I A&B) of the $LL37_{FRRV}$ peptide variants were mixed with PTAA. As the net charge of the peptide increased from 0 to +2 for the acetyl-capped peptide variants and from +1 to +3 for the uncapped peptide variants, a corresponding increase in PTAA's fluorescence intensity was observed (Figure 3A). UV/Vis absorption data (Figure S3.II A–F) was in agreement with the trends observed with fluorescence data, in that, the magnitude of the blue-shift in absorption upon peptide addition correlated with the peptide's net charge. Overall, these results emphasize that the number of positive charges on the intact peptide directly affected PTAA's fluorescence intensity.

Additionally, when PTAA was mixed with any of the six different $LL37_{FRRV}$ peptide variants (Table 1, seq ID 1–6) after they were treated with OmpT to allow digestion of the peptides into their respective shorter cleaved fragments, the fluorescence intensity decreased by ≈5–70% in comparison to the intact peptide (Figure 3B and Figure S3.I C). The reason for this difference in fluorescence intensity between cleaved and intact peptides is explained in the previous section. However, what's interesting to note is that, even though the fragments have similar or higher charge than the intact peptide (Table 1a & b), the longer intact peptide always shows a higher fluorescence intensity than the fragments (Figure S3.I C, dark hues vs. lighter hues). It implies that the peptide length has a relatively stronger influence on PTAA fluorescence intensity than the positive charges on the peptide, at least for the 15-mer peptides tested here. As expected, the magnitude of difference in PTAA fluorescence intensity between the cleaved and intact peptides for the six $LL37_{FRRV}$ variants was different (Figure 3B). This is due to a combination of different factors including the peptide's net charge, the accompanying minor change to the peptide sequence, and the difference in OmpT's preference for each of the six peptides. Notably, the peptide with zero net charge showed very little difference in PTAA fluorescence intensity (Figure 3B brown bar 0). However, as the peptide's net charge increased from +1 to +3, there was a corresponding increase in the magnitude of difference in PTAA fluorescence (Figure 3B). Intact $LL37_{FRRV}$, with the highest net positive charge of +3 showed the largest difference in fluorescence intensity (Figure 3B red bar +3). In the context of the OmpT-PTAA assay described below, $LL37_{FRRV}$ is indeed the optimal peptide as it provides the largest window of change between the intact and cleaved peptide.

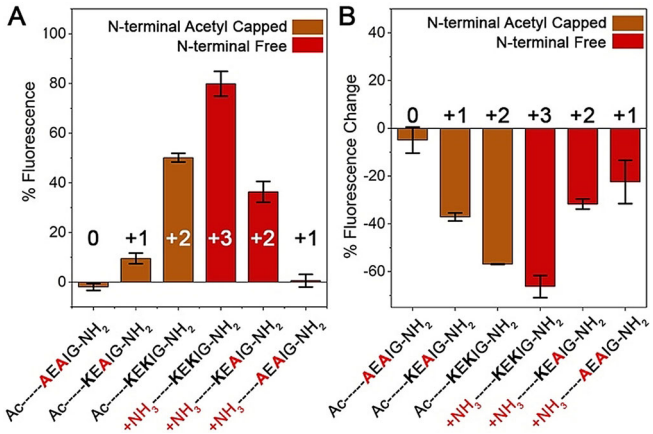

Figure 3. Effect of peptide net charge on PTAA fluorescence intensity. A) Fluorescence intensity of PTAA when mixed with 6.25 μM of $LL37_{FRRV}$ peptide variants of different net charge (Table 1 ID 1–6). The peptide's N-terminal was either acetyl capped (brown) or left unmodified (red). B) Difference in PTAA fluorescence intensity (plotted as % fluorescence change) between cleaved and intact peptides resulting from OmpT digestion (for details, see Section S3.I C). Short dashes in the X-axis labels indicate the constant N-terminal portion (CLLGDFFRRV) of the $LL37_{FRRV}$ peptide variants listed in Table 3. The numbers within and above the vertical bars indicate net charge of the peptide. Error bars represent standard error of the mean for $n=3$.

A third factor affecting PTAA fluorescence when mixed with $LL37_{FRRV}$ is the distribution of positive charges along the peptide sequence. The peptide's positively charged amino groups may act as contact points that help anchor the peptide onto the negatively charged carboxyl group of the polymer side chains. The position, distance, and regularity of such contact points along a continuous stretch of the peptide can determine the extent to which the peptide effectively induces chirality of the PTAA backbone. Additional $LL37_{FRRV}$ peptide variants (Table 2 ID 3,7–9) were designed such that their positive charges were distributed along the sequence without altering their net charge. When mixed with PTAA, the charge distributed peptides caused an increase in PTAA fluorescence and exhibited a blue-shift in their absorption (Figure S3.I E and S3.II G–I, respectively). See section S3.I and S3.II in the supplementary info file for details. However, there was no clear trend in the increase in PTAA fluorescence when the maximum distance between any two positive charges on the peptide sequence was varied between 11, 10, 8, and 6 residues (Figure S3.I E&F), except when the phenylalanine next to the optimized FRRV sequence was replaced by lysine (Table 2 ID 9). This does not necessarily

Table 2: List of $LL37_{FRRV}$ peptide variants with positive charge distributed along the sequence; net charge (a).

ID	Peptide Sequence	*a*	Number of residues between peripheral positive charges
3	$^{+}NH_3$-CLLGDFFRRVKE**K**IG-NH_2	+3	11
7	Ac-C**K**LGDFFRRVKE**K**IG-NH_2	+3	10
8	Ac-CLL**K**DFFRRVKE**K**IG-NH_2	+3	8
9	Ac-CLLGD**K**FRRVKE**K**IG-NH_2	+3	6

mean that the charge distribution is not a significant factor in affecting PTAA fluorescence, but instead hints at the interplay of additional associated factors such as the propensity to fold into secondary conformations which are known to be governed by the peptide sequence.

The interactions between PTAA and the intact and cleaved peptides, in the context of secondary conformation, will be addressed below using CD spectroscopy.

Characterization of Secondary Conformation of PTAA, Intact/Cleaved $LL37_{FRRV}$, and Their Interactions

Polythiophenes are known to show split-type induced CD (ICD) in the π-π* transition region (320–500 nm).[34,35] CD spectra of PTAA in a pH 8 reaction buffer suggests PTAA is optically inactive as it does not exhibit any characteristic ICD pattern in the π-π* transition region (Figure 4A black). The absence of CD signal as well as an absorption maximum at 450 nm (Figure 2A black) confirms that PTAA backbone adopts a planar achiral conformation in the pH 8 reaction buffer. However, upon adding $LL37_{FRRV}$, split-type ICDs in the π-π* transition region is evident (Figure 4A blue). Collectively, the blue shift in absorption, increase in PTAA's fluorescence upon $LL37_{FRRV}$ addition, and ICD for PTAA-$LL37_{FRRV}$, indicate that a helical structure is induced in PTAA backbone due to the interaction between PTAA and $LL37_{FRRV}$ (Figure 2A,B, and Figure 4A blue). In addition, the shape and sign of the ICD pattern for PTAA indicates that it is a left-handed helical form of PT.[34,36]

In the absence of PTAA, the CD spectra of samples containing (1) $LL37_{FRRV}$, (2) OmpT cleaved $LL37_{FRRV}$ fragments, or (3) $_{frag1}LL37_{FRRV}$ and $_{frag2}LL37_{FRRV}$ did not exhibit any defined secondary conformation (Figure 4A red, magenta, and orange). However, in the presence of PTAA, $LL37_{FRRV}$ adopted a right-handed α-helical secondary conformation as interpreted from the characteristic negative CD bands at 222 and 208 nm of equal intensities, and a strong positive band at 192 nm (Figure 4A blue). Similar observations of initially unstructured peptides undergoing conformational changes upon interacting with PTs have been reported earlier.[17,18] The conformational change observed in $LL37_{FRRV}$ is also reminiscent of the full length LL37, which is known to adopt helical conformation when exposed to negatively charged assemblies, like lipid membranes.[13,14] Meanwhile, in the presence of PTAA, OmpT cleaved $LL37_{FRRV}$ fragments and $_{frag1}LL37_{FRRV}$ and $_{frag2}LL37_{FRRV}$ did not exhibit any defined secondary conformation, and nor did PTAA itself, when mixed with the above fragments (Figure 4A green and purple). Further characterization of $_{frag1}LL37_{FRRV}$ and $_{frag2}LL37_{FRRV}$ revealed that the individual fragments remain largely random coil in the absence of PTAA (Figure S4). The above CD data clearly confirms that the interactions between PTAA and the cleaved and synthesized fragments, if any, are weak and unable to force PTAA to adopt a helical and chiral conformation with a distinct optical response (Figure 4A and 2H–J). A pictorial summary of the possible interactions between PTAA and cleaved/uncleaved peptide substrates is shown in Figure 4B. It is worthwhile emphasizing that the exact interactions between a peptide and polythiophene are unresolved and still debated in the literature.[18,28]

Dynamic light scattering (DLS) and atomic force microscopy (AFM) were employed to further investigate potential interactions between PTAA and $LL37_{FRRV}$ and its fragments. DLS data of PTAA samples indicated formation of polydisperse sub-micron assemblies that became relatively less polydisperse upon addition of $LL37_{FRRV}$ (Figure S6 A black

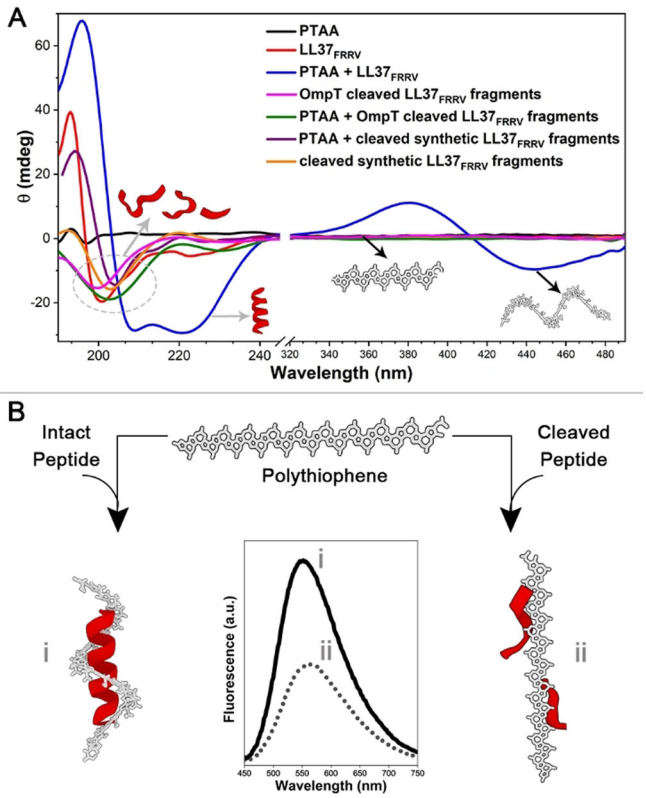

Figure 4. Secondary structure characterizations. A) CD measurements of PTAA, $LL37_{FRRV}$, PTAA-$LL37_{FRRV}$ complex, OmpT cleaved $LL37_{FRRV}$ fragments, PTAA mixed with OmpT cleaved $LL37_{FRRV}$ fragments, PTAA mixed with synthetic cleaved $LL37_{FRRV}$ fragments, and cleaved synthetic $LL37_{FRRV}$ fragments. B) Schematic illustration of the proposed mechanism of PTAA-peptide interaction in the presence and absence of OmpT. (i) Intact $LL37_{FRRV}$ and PTAA interact electrostatically and both molecules adopt a helical conformation. (ii) $LL37_{FRRV}$ cleaved by OmpT in detergent micelles may interact with PTAA without inducing any structural changes. Center panel illustrates the fluorescence intensity changes in PTAA corresponding to the scenarios in (i) and (ii).

and blue line). Such a response was absent when the cleaved fragments were mixed with PTAA (Figure S6 A purple line). AFM imaging qualitatively supports DLS measurements (Figure S6 B–D). However, the size of the assemblies observed were not consistent with those seen in DLS measurements. This is most likely due to artefacts resulting from the drying process. Overall, DLS, AFM, CD, UV/Vis, and fluorescence data are in qualitative agreement suggesting that PTAA undergoes changes (physical, conformational, or optical) only in the presence of the intact peptide, but not when mixed with the cleaved fragments.

Taken together, our efforts to gain deeper mechanistic understanding of interactions between PTAA and peptides reveal that even small changes to the peptide sequence can have profound influence on PTAA's optical properties due to the interplay of multiple factors. However, by investigating the effect of peptide length, net charge, distribution of positive charges along the peptide sequence, minor changes to the sequences, and the ability to adopt a well-defined secondary conformation, we have identified two factors—peptide length and net positive charge—as the major factors that influence PTAA conformation, conjugation length, chirality and its fluorescence properties when interacting with $LL37_{FRRV}$ and its peptide variants.

A Method to Detect E. coli *Wild-Type Strains using PTAA and* $LL37_{FRRV}$

The ability of PTAA to distinguish between an intact $LL37_{FRRV}$ and its cleaved fragments was exploited to develop an assay for detecting *E. coli* in water samples. Unlike previously reported *E. coli* detection methods that rely on electrostatic interactions between cationic peptides and oppositely charged bacterial surfaces, targeting OmpT's proteolytic activity for *E. coli* detection has the benefit of specificity.[37] For this, we employed four different strains of *E. coli* (Table S2): BL21, K12 (ATCC® 700926™), J96 and Lemo21(DE3). BL21 acted as a negative control as this strain lacks the genes necessary to synthesize OmpT and therefore does not have any OmpT present on its outer membrane. K12 and J96 are two wild-type strains of *E. coli* expressing OmpT on the outer membrane, with the latter strain expressing OmpT at a slightly higher level. A Lemo21(DE3) strain overexpressing recombinant OmpT on the outer membrane was used as a positive control. See experimental section in supplementary file for details.

Water samples were spiked with 10^8, 10^7 and 10^6–10^3 CFU mL^{-1} *E. coli* and filtered through a 0.2 μm PTFE filter to concentrate the *E. coli* cells. For high *E. coli* concentrations (10^8 CFUs mL^{-1}), a starting sample volume of 200 μL was sufficient, but the volume had to be increased to 2 mL and 20 mL for 10^7 and 10^6–10^3 CFUs mL^{-1}, respectively. The *E. coli* concentrates were suspended in 90 μL of the reaction buffer to which 10 μL of 500 μM $LL37_{FRRV}$ was added. After incubation for 1 h at 37 °C to allow the *E. coli* cells to interact with and cleave $LL37_{FRRV}$, PTAA was added and the fluorescence intensity at 550 nm was recorded. For the sake of convenience, we call this approach the "Pre-concentration method" (Figure 5 A top panel).

Results show a significant reduction in PTAA's fluorescence intensity for samples containing K12, J96, and Lemo21-(DE3) strains, suggesting that these *E. coli* strains were able to cleave $LL37_{FRRV}$ (Figure 5 B blue, red, and magenta). Control samples containing the *E. coli* BL21 strain did not show any reduction in PTAA's fluorescence intensity (Figure 5 B black). Moreover, the reduction in PTAA's fluorescence is consistent with the different levels of OmpT expression on the surface of different *E. coli* strains. This was also confirmed in a separate FRET-based kinetic study (Figure S7).

Although it is tempting to exploit this differential OmpT expression to distinguish between specific strains of *E. coli*, we do not consider surface OmpT levels as a reliable marker since protein expression levels are influenced by the bacteria's environment and growth stage.[38] For the two wild-type strains, K12 and J96, the limit of detection (LOD) which we define as a 20 % change in fluorescence intensity, is 10^5 and 10^6 CFU mL^{-1}, respectively (Figure 5 B blue and red). The ability to detect *E. coli* in highly contaminated water samples

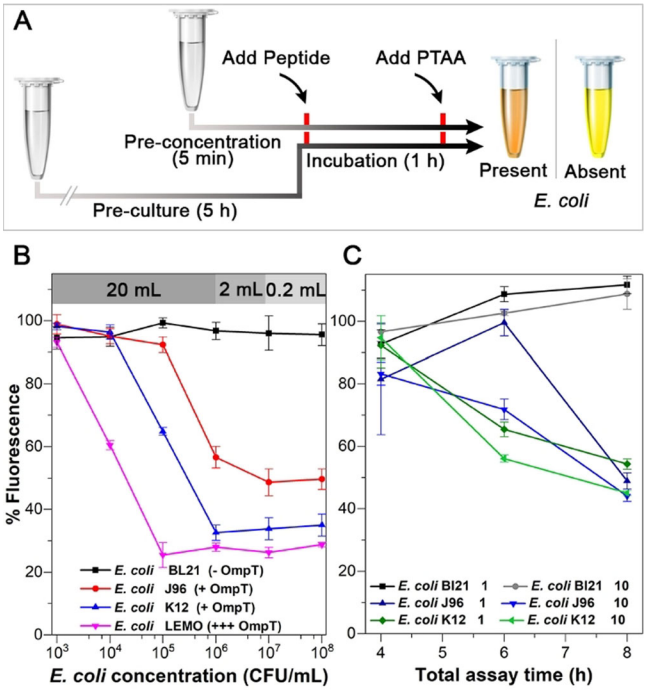

Figure 5. *E. coli* detection. A) Approaches to *E. coli* sensing using PTAA-$LL37_{FRRV}$: (Top) *E. coli* sensing using the pre-concentration method, (Bottom) *E. coli* sensing using the pre-culture method. B) Detection of different strains of *E. coli*. Fluorescence intensity of PTAA when mixed with $LL37_{FRRV}$ treated with different *E. coli* strains while using the pre-concentration method. 200 μL (light grey), 2 mL (grey) and 20 mL (dark grey) of sample volumes were used for detecting 10^8, 10^7, 10^6–10^3 CFU mL^{-1} of *E. coli*, respectively. C) Fluorescence intensity of PTAA when mixed with $LL37_{FRRV}$ treated with *E. coli* K12 or J96 wildtype strains using pre-culture method for detecting 1 and 10 CFU mL^{-1} of *E. coli*. Data in B & C were normalized for the highest PTAA fluorescence intensity at 550 nm and plotted as % fluorescence. Error bars in B & C indicate standard error of the mean for data points averaged from duplicates for $n = 3$.

within an hour is extremely useful for on-site applications. However, these are without doubt high *E. coli* concentrations and it would be much more useful to develop strategies that enable detection of significantly lower levels of *E. coli* contaminated samples.

Detection of E. coli *at 1–10 CFU mL^{-1} using a Pre-culture Step*

In order to improve the LOD, we repeated the experiment with the two wild-type strains, K12 and J96, while introducing a pre-culture step. For the sake of convenience, we call this approach the "Pre-culture method" (Figure 5A bottom panel). In this method, water samples spiked with *E. coli* at 1 and 10 CFU mL^{-1} cells were first cultured in LB media for up to 7 h. 200 μL of this pre-cultured sample was then analyzed by following the steps described in the pre-concentration method above. Results indicate that PTAA's fluorescence intensity at 550 nm reduced by almost 35% and 44% for 1 and 10 CFUs mL^{-1} of K12 strain, respectively, when pre-cultured for only 5 h (Figure 5C dark and light green). Similarly, a reduction in PTAA's fluorescence intensity of 28% was observed for 10 CFUs mL^{-1} of J96 strain when pre-cultured for 5 h (Figure 5C magenta). It took 8 h of pre-culturing to detect 1 CFU mL^{-1} of the J96 strain which showed a reduction of PTAA's fluorescence intensity of almost 51% (Figure 5C light blue). In other words, by using the pre-culture method of detection, as low as 1 CFU mL^{-1} of K12 *E. coli* can be detected within 6 h. For J96, the *E. coil* strain commonly seen in urine samples of patients suffering from urinary tract infections, 1 CFU mL^{-1} can be detected within 8 h. Meanwhile, PTAA mixed with $LL37_{FRRV}$ exposed to BL21 cells lacking surface OmpT did not exhibit a reduction in fluorescence (Figure 5C black and grey). The slight increase in fluorescence observed at the end of 6 and 8 h, respectively, is likely due to changes in the growth media during the course of the assay when cells continue to grow (Figure S8). Thus, the proposed assay works well for analyzing water samples where there is very little interference from the sample matrix. However, it might become necessary to include a pre-processing step for samples with complex matrices such as biological fluids and food samples.

Using the method described above, we were able to detect *E. coli* in highly contaminated samples within 1 h, and with the use of a pre-culturing step, we improved the assay detection limit in weakly contaminated samples to detect as low as 1 or 10 CFU mL^{-1} in as little as 6–8 h. This is a significant achievement because most commercially available kits require about 2–3 fold longer assay time to detect 1 CFU mL^{-1} of *E. coli*.[39–45] In Table 3, we benchmark the proposed method in terms of LOD and assay time against a few existing kits (a comprehensive comparison of the OmpT-PTAA method with commercial kits and published research methods is summarized in Figure S9 and S10). Additionally, storage benefits governed by the use of highly robust materials (polymer and peptide), simplicity and ease of use, and overall cost offer opportunities to translate the assay into a viable test format for applications near outbreaks and in resource-limited regions.

Table 3: Selected list of commercially available *E. coli* detection kits.

Product, *Company*	Assay Type	LOD	Assay Time[a]	Storage
RapidChek *E. coli* O157 Romer Labs[39]	Selective enrichment media and LFI	N.A.	8–18 h	RT
AquaVial *Aquabsafe*[40]	Colorimetric (Enzyme)	1 CFU mL^{-1}	≈24 h	N.A.
MicroSnap™ *E. coli* Test Kit *Hygiena*[41]	Bioluminogenic substrate	< 10 CFU	8 h	N.A.
Drinking Water Test Kit *Rakiro*[42]	Colorimetric (Enzyme)	1 CFU cL^{-1}	18–24 h	RT
Compartment Bag Test *Aquagenx*[43]	Colorimetric	N.A.	24–48 h	RT
Colilert *IDEXX*[44]	Enzyme	N.A.	≈24 h	RT
Solus *E. coli* O157 ELISA *Solus Scientific*[45]	ELISA	10^4–10^5 CFU mL^{-1}	18–22 h	2–8 °C

[a] Assay time, including any incubation steps involved.

Conclusion

We report a simple yet sensitive method to detect very low levels of *E. coli* in water by targeting the bacteria's surface protease activity. To the best of our knowledge, this is the first time, an outer-membrane protease in conjugation with an unlabeled peptide has been targeted to develop a functional assay for *E. coli* detection. In this method, PTAA was employed as a reporter capable of distinguishing between an intact and cleaved peptide that was previously optimized for OmpT. Characterization of PTAA-peptide interactions helped identify net charge and peptide length (and indirectly the secondary conformation) as important factors that affect PTAA structural and optical properties when interacting with the intact and cleaved peptides. In combination with our previous study on optimizing peptides for OmpT,[11] we have gained significant insights into OmpT-peptide and peptide-PTAA interactions which helped us design cationic peptides for *E. coli* detection that were not only optimized for catalytic activity, but also for optimal reporting. Using this method, we were able to detect as low as 1 CFU mL^{-1} of the K12 and J96 wild-type *E. coli* strains in water within a total assay time of 6 and 8 h, respectively. These assay times are significantly

shorter than most commercially available detection kits for *E. coli*.

The OmpT based approach for *E. coli* detection utilizing protease specific substrates can be developed into a test kit that can easily be extended to other bacteria expressing similar outer-membrane proteases e.g., *Salmonella*, *Y. pestis*, etc. By identifying substrate sequences that are exclusive to each protease, it is possible to design assays capable of detecting multiple bacteria in a sample. Development of such multiplexed detection strategies based on protease substrate specificity is currently under way and will be reported elsewhere.

Acknowledgements

This work was funded by the Singapore Ministry of Education Academic Research Fund Tier 2 (MOE2018-T2-1-025) and the NTU-NU Institute for NanoMedicine located at the International Institute for Nanotechnology, Northwestern University, USA and the Nanyang Technological University, Singapore; Agmt10/20/14. We thank Ms. Batika Saxena for help with the graphics.

Conflict of interest

The authors declare no conflict of interest.

Keywords: enzymes · fluorescence · membrane proteins · pathogens · peptides

[1] WHO, WHO Estimates of the Global Burden of Foodborne Diseases, World Health Organization, **2015**.
[2] Y. Wang, J. K. Salazar, *Compr. Rev. Food Sci. Food Saf.* **2016**, *15*, 183 – 205.
[3] O. Lazcka, F. J. Del Campo, F. X. Muñoz, *Biosens. Bioelectron.* **2007**, *22*, 1205 – 1217.
[4] J. W.-F. Law, N.-S. Ab Mutalib, K.-G. Chan, L.-H. Lee, *Front. Microbiol.* **2015**, *5*, 770.
[5] V. Hritonenko, C. Stathopoulos, *Mol. Membr. Biol.* **2007**, *24*, 395 – 406.
[6] N. Dekker, *Handbook of Proteolytic Enzymes*, Elsevier, Amsterdam, **2013**, pp. 284 – 289.
[7] R. A. Kramer, D. Zandwijken, M. R. Egmond, N. Dekker, *Eur. J. Biochem.* **2000**, *267*, 885 – 893.
[8] N. Dekker, R. C. Cox, R. A. Kramer, M. R. Egmond, *Biochemistry* **2001**, *40*, 1694 – 1701.
[9] S. Stumpe, R. Schmid, D. L. Stephens, G. Georgiou, E. P. Bakker, *J. Bacteriol.* **1998**, *180*, 4002 – 4006.
[10] C.-Y. Hui, Y. Guo, Q.-S. He, L. Peng, S.-C. Wu, H. Cao, S.-H. Huang, *Microbiol. Immunol.* **2010**, *54*, 452 – 459.
[11] S. E. Wood, G. Sinsinbar, S. Gudlur, M. Nallani, C.-F. F. Huang, B. Liedberg, M. Mrksich, *Angew. Chem. Int. Ed.* **2017**, *56*, 16531 – 16535; *Angew. Chem.* **2017**, *129*, 16758 – 16762.
[12] A. A. Bahar, D. Ren, *Pharmaceuticals* **2013**, *6*, 1543 – 1575.
[13] U. H. N. Dürr, U. S. Sudheendra, A. Ramamoorthy, *Biochim. Biophys. Acta Biomembr.* **2006**, *1758*, 1408 – 1425.
[14] G. Wang, *J. Biol. Chem.* **2008**, *283*, 32637 – 32643.
[15] K. Lee, L. K. Povlich, J. Kim, *Analyst* **2010**, *135*, 2179 – 2189.
[16] S. Das, P. Routh, R. Ghosh, D. P. Chatterjee, A. K. Nandi, *Polym. Int.* **2017**, *66*, 623 – 639.
[17] K. P. R. Nilsson, M. R. Andersson, O. Inganäs, *J. Phys. Condens. Matter* **2002**, *14*, 10011 – 10020.
[18] K. P. R. Nilsson, J. Rydberg, L. Baltzer, O. Inganäs, *Proc. Natl. Acad. Sci. USA* **2004**, *101*, 11197 – 11202.
[19] D. Raithel, L. Simine, S. Pickel, K. Schötz, F. Panzer, S. Baderschneider, D. Schiefer, R. Lohwasser, J. Köhler, M. Thelakkat, et al., *Proc. Natl. Acad. Sci. USA* **2018**, *115*, 2699 – 2704.
[20] K. P. R. Nilsson, J. Rydberg, L. Baltzer, O. Inganas, *Proc. Natl. Acad. Sci. USA* **2003**, *100*, 10170 – 10174.
[21] M. Leclerc, K. Faïd, *Adv. Mater.* **1997**, *9*, 1087 – 1094.
[22] K. Faïd, M. Leclerc, *J. Am. Chem. Soc.* **1998**, *120*, 5274 – 5278.
[23] S. E. Domínguez, M. Cangiotti, A. Fattori, T. Ääritalo, P. Damlin, M. F. Ottaviani, C. Kvarnström, *Langmuir* **2018**, *34*, 7364 – 7378.
[24] Y. Wu, Y. Tan, J. Wu, S. Chen, Y. Z. Chen, X. Zhou, Y. Jiang, C. Tan, *ACS Appl. Mater. Interfaces* **2015**, *7*, 6882 – 6888.
[25] T. Shiraki, A. Dawn, Y. Tsuchiya, S. Shinkai, *J. Am. Chem. Soc.* **2010**, *132*, 13928 – 13935.
[26] R. D. McCullough, P. C. Ewbank, R. S. Loewe, *J. Am. Chem. Soc.* **1997**, *119*, 633 – 634.
[27] B. Kim, L. Chen, J. Gong, Y. Osada, *Macromolecules* **1999**, *32*, 3964 – 3969.
[28] R. Selegård, Z. Rouhbakhsh, H. Shirani, L. B. G. Johansson, P. Norman, M. Linares, D. Aili, K. P. R. Nilsson, *Macromolecules* **2017**, *50*, 7102 – 7110.
[29] H. Lu, C. Zhou, X. Zhou, H. Sun, H. Bai, Y. Wang, F. Lv, L. Liu, Y. Ma, S. Wang, *Adv. Electron. Mater.* **2017**, *3*, 1700161.
[30] X. Chen, H. Guan, Z. He, X. Zhou, J. Hu, *Anal. Methods* **2012**, *4*, 1619 – 1622.
[31] P. Åsberg, P. Björk, F. Höök, O. Inganäs, *Langmuir* **2005**, *21*, 7292 – 7298.
[32] K. F. Karlsson, P. Åsberg, K. Peter, R. Nilsson, O. Inganäs, *Chem. Mater.* **2005**, *17*, 4204 – 4211.
[33] J. Rubio-Magnieto, E. G. Azene, J. Knoops, S. Knippenberg, C. Delcourt, A. Thomas, S. Richeter, A. Mehdi, P. Dubois, R. Lazzaroni, D. Beljonne, et al., *Soft Matter* **2015**, *11*, 6460 – 6471.
[34] K. P. R. Nilsson, J. D. M. Olsson, P. Konradsson, O. Inganäs, *Macromolecules* **2004**, *37*, 6316 – 6321.
[35] E. Yashima, T. Matsushima, Y. Okamoto, *J. Am. Chem. Soc.* **1997**, *119*, 6345 – 6359.
[36] H. Goto, Y. Yokochi, E. Yashima, *Chem. Commun.* **2012**, *48*, 3291 – 3293.
[37] J. Han, H. Cheng, B. Wang, M. S. Braun, X. Fan, M. Bender, W. Huang, C. Domhan, W. Mier, T. Lindner, et al., *Angew. Chem. Int. Ed.* **2017**, *56*, 15246 – 15251; *Angew. Chem.* **2017**, *129*, 15448 – 15453.
[38] J.-L. Thomassin, J. R. Brannon, B. F. Gibbs, S. Gruenheid, H. Le Moual, *Infect. Immun.* **2012**, *80*, 483 – 492.
[39] "E. coli O157 Test Kits | Fast & reliable E. coli O157 detection," can be found under https://www.romerlabs.com/en/analytes/food-pathogens/e-coli/, (accessed Jun 13, **2020**).
[40] "AquaVial Water Test Kit—E. Coli and Coliform—AquaBSafe," can be found under https://www.aquabsafe.com/products/aquavial-water-test-kit-e-coli-and-coliform, (accessed Jun 13, **2020**).
[41] "MicroSnap E. coli—Hygiena," can be found under https://www.hygiena.com/microsnap-e-coli-other.html, (accessed Jun 13, **2020**).
[42] "Drinking Water Test Kit (E.coli/ Coliform Test)—Rakiro," can be found under https://rakiro.net/product/bacteria-testing-kits/drinking-water-test-kit-e-coli-coliform-test/, (accessed Jun 13, **2020**).
[43] "Aquagenx ® CBT EC + TC (Compartment Bag Test)," can be found under https://www.aquagenx.com/wp-content/uploads/2019/09/MPN-CBT-ECTC-Instructions-DrinkingWater-Sept2019.pdf, (accessed Jun 13, **2020**).

Research Articles

Enzymes

G. Sinsinbar, S. Gudlur, S. E. Wood, G. Ammanath, H. U. Yildiz, P. Alagappan, M. Mrksich, B. Liedberg* ▬ ▮▮▮▮–▮▮▮▮

Outer-Membrane Protease (OmpT) Based *E. coli* Sensing with Anionic Polythiophene and Unlabeled Peptide Substrate

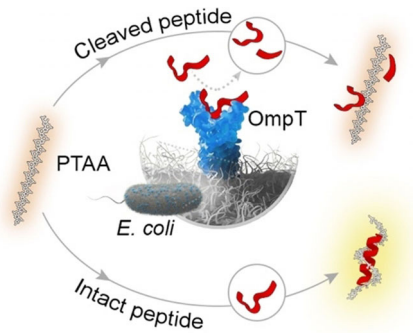

The structural and optical changes resulting from the interaction between a polythiophene (PTAA) and a short unlabeled peptide were exploited to develop a sensitive bacterial detection method. The method itself targets the bacteria's surface protease activity and is sensitive enough to detect 1 CFU mL^{-1} of *E. coli* in water within 6 hours.

Enzymes

G. Sinsinbar, S. Gudlur, S. E. Wood, G. Ammanath, H. U. Yildiz, P. Alagappan, M. Mrksich, B. Liedberg* ▬ ▮▮▮▮–▮▮▮▮

Outer-Membrane Protease (OmpT) Based *E. coli* Sensing with Anionic Polythiophene and Unlabeled Peptide Substrate

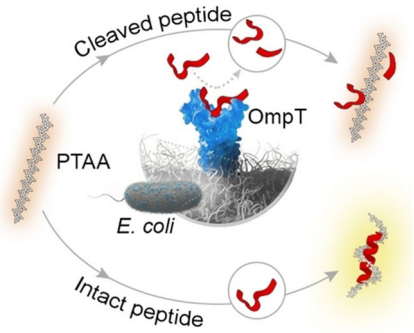

The structural and optical changes resulting from the interaction between a polythiophene (PTAA) and a short unlabeled peptide were exploited to develop a sensitive bacterial detection method. The method itself targets the bacteria's surface protease activity and is sensitive enough to detect 1 CFU mL^{-1} of *E. coli* in water within 6 hours.

Research Articles

Enzymes

G. Sinsinbar, S. Gudlur, S. E. Wood, G. Ammanath, H. U. Yildiz, P. Alagappan, M. Mrksich, B. Liedberg* ____ ▮▮▮▮–▮▮▮▮

Outer-Membrane Protease (OmpT) Based *E. coli* Sensing with Anionic Polythiophene and Unlabeled Peptide Substrate

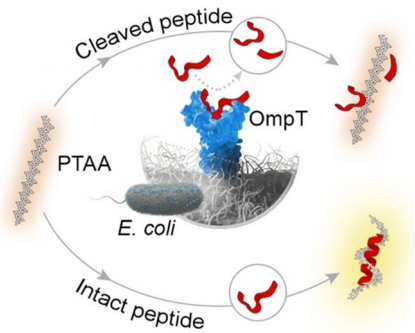

The structural and optical changes resulting from the interaction between a polythiophene (PTAA) and a short unlabeled peptide were exploited to develop a sensitive bacterial detection method. The method itself targets the bacteria's surface protease activity and is sensitive enough to detect 1 CFU mL^{-1} of *E. coli* in water within 6 hours.

These are not the final page numbers!